On the Rate Control and Information Exchange for Optimizing Data Transfers in IPNs

Xiaojian Tian, Xiaoliang Chen, Xixuan Zhou, Nirwan Ansari, *Fellow, IEEE*, and Zuqing Zhu, *Fellow, IEEE*

***Abstract*—Recently, the growing of deep space explorations has attracted notable interests on interplanetary network (IPN), which is the key infrastructure for communications across vast distances in the solar system. However, the unique characteristics of IPN pose numerous unexplored challenges for interplanetary data transfers (IP-DTs), *i.e.*, the challenges that existing schemes developed for Earth-based networks are ill-equipped to handle. To address these challenges, we first propose a novel distributed algorithm that leverages the Lyapunov optimization to jointly optimize the routing, scheduling and rate control of IP-DTs at each node. Specifically, our proposal adaptively optimizes the data-rate and bundle scheduling at each output port of a node, significantly improving the end-to-end (E2E) latency and delivery ratio of IP-DTs under a long-term energy constraint. Then, we further explore the heterogeneity of IPN to introduce limited state information exchange among nodes, and devise mechanisms for generating and disseminating state messages to facilitate timely adjustments of routing and scheduling schemes in response to unexpected link disruptions and traffic surges. Simulations verify the advantages of our proposal over the state-of-the-arts.**

***Index Terms*—Interplanetary networks, Distributed routing and data scheduling, Rate control, Information exchange.**

I. Introduction

In recent years, there has been a notable increase in global interest in deep space and planetary exploration [1]. A number of missions have been launched or are in preparation, *e.g.*, China's Moon and Mars exploration missions [2, 3], the National Aeronautics and Space Administration's (NASA's) Europa Clipper [4] and asteroid sampling [5] missions, and the European Space Agency's Jupiter icy moons explorer and planetary defense missions [6]. The surge of such missions underscores the crucial role of the network infrastructure that enables interplanetary communications, leading to the studies on interplanetary networks (IPNs) [7]. Specifically, IPN facilitates reliable data exchanges among various deep space objects (*e.g.*, satellites, rovers, spacecrafts and ground stations) [8], and covers multiple celestial bodies as shown in Fig. 1. Despite its origins decades ago, IPN research remains highly relevant today, as ongoing deep space missions bring new challenges, such as increased traffic loads, longer queuing delays, and higher energy consumption.

IPNs are currently relatively small in scale, *i.e.*, the number of nodes in an existing IPN is usually smaller than 20. This is because these IPNs were normally architected for individual deep space exploration missions. For example, the IPN built for China's Chang'e-5 mission [2] only consists of fewer than 10 nodes, including the orbiter, lander, ascender, Queqiao relay satellite and ground receiving stations. However, we anticipate a rapid increase in their nodes and links in the near future, driven by the aggressively-growing projects related to manned exploration of Moon [9], permanent Moon bases [10, 11], Mars immigration [12], *etc*. This will not only expand the scale of IPN but also increase the volume and variety of IPN traffic [13], posing unexplored challenges for the routing and scheduling of interplanetary data transfers (IP-DTs).

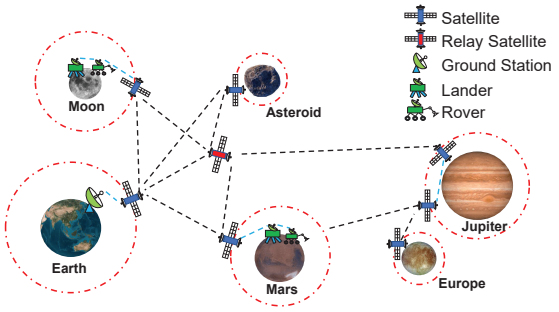

Fig. 1. An example of IPN.

Compared with other known networks [14–24], IPN is unique from several perspectives, rendering the routing and data scheduling schemes developed for networks on/around Earth inapplicable to it. For instance, low Earth orbit (LEO) satellite networks often rely on existing network protocols like TCP, and do not require extreme resilience and flexibility, owing to their shorter communication latencies (at millisecond level), better connectivity, and lower error rates. First, the vast distances between celestial bodies lead to extremely long IPN links, and their movements and shields result in intermittent connections and much more dynamic IPN topologies. This overrules the possibility of centralized network control or end-to-end routing path planning. Hence, while studies on LEO satellite networks assumed short and predictable transmission delays to leverage existing protocols [25–27], IPNs face unique challenges that make precise coordination of routing, data scheduling and rate control with brand-new techniques necessary. Second, IPN is intrinsically much more heterogeneous than other known networks, due to the huge differences (in several orders of magnitude) in links, and computing/storage capacities and power budgets of nodes. Third, most IPN nodes (*e.g.*, satellites and rovers) only have very limited computing/storage capacities and power budgets (*i.e.*, solar power

X. Tian, X. Chen, X. Zhou and Z. Zhu are with the School of Information Science and Technology, University of Science and Technology of China, Hefei, Anhui 230027, P. R. China (email: xlichen@ieee.org, zqzhu@ieee.org).

N. Ansari is with the Advanced Networking Laboratory, Department of Electrical and Computer Engineering, New Jersey Institute of Technology, Newark, NJ 07102, USA (email: nirwan.ansari@njit.edu).

Manuscript received on September 13, 2024.

is the only available power source) [28], which precludes the execution of complex routing and scheduling algorithms. Lastly, the extreme electromagnetic (EM) interference prevalent in deep space often induces sudden and unpredictable interruptions in IPN communications [29], posing significant challenges in ensuring reliable IP-DTs.

Currently, the study of routing and data scheduling in IPN is still immature, and thus existing approaches in the literature can hardly address the aforementioned challenges properly. Initially, NASA proposed to divide data into bundles (*i.e.*, atomic data blocks for IP-DTs) and introduced a contact graph routing (CGR) approach [30] to plan the routing schemes of these bundles, but these proposals overlooked the buffering and scheduling of bundles in each IPN node. Later on, a few proposals were reported in [31–35] to optimize the routing planning of CGR in consideration of how bundles are queued in IPN nodes. However, all these approaches processed bundles in each queue in the first-in-first-out (FIFO) manner, without considering bundle-level scheduling in IPN nodes. More recently, studies in [36–39] designed algorithms to optimize the routing and scheduling of bundles in each IPN node independently. Nevertheless, the state-of-the-arts in [36–39] failed to address or leverage the heterogeneity of IPN. While there are few studies on queue scheduling in DTNs with deterministic contact schedules, our work fills this gap by introducing a framework that jointly optimizes routing, data scheduling, and rate control in IPNs, addressing the unique challenges of energy constraints, extremely long delays, *etc*.

Note that, the performance of routing and data scheduling of IP-DTs can be further improved from at least two aspects by considering the heterogeneity of IPN. First, as the lengths of links from a same IPN node can vary in several orders of magnitude (*e.g.*, a satellite orbiting Mars may communicate with both a rover on Mars and another satellite around Earth), optimizing the data-rate of each link connection adaptively can improve routing and data scheduling in the node, along with enhancing energy-efficiency. However, all studies in [36–39] assumed that the data-rate of each link in a contact is constant and not adjustable. Second, due to the substantial differences in link lengths, it may be impractical to exchange state information between IPN nodes when the link between two nodes is exceptionally long (*e.g.*, between Earth and Mars), considering the loss of timeliness. By only considering the routing of IP-DTs, researchers have verified the benefits of limited state information exchange in [32, 40], but approaches in [36–39] completely disregarded state information exchange.

The main contributions of this work are as follows:

- We formulate a detailed model that jointly optimizes the routing, scheduling and rate control of IP-DTs on each IPN node under a power budget.
- We propose an effective algorithm by leveraging Lyapunov optimization [41], with a customized adaptation that includes a penalty function and problem decomposition tailored specifically based on the features of IPNs.
- We introduce limited state information exchange and devise an approach to adjust routing and data scheduling in IPN nodes timely in response to unexpected link interruptions and traffic increase on neighboring nodes.
- We validate the advantages of our proposals through extensive simulations, demonstrating its effectiveness over existing benchmarks.

The rest of the paper is organized as follows. In Section II, we provide an overview of IPN and survey the related work briefly. Section III details the optimization model and presents the Lyapunov-based algorithm devised to solve it. The limited state information exchange mechanism is introduced in Section IV. Our proposals are evaluated through simulations in Section V. Finally, Section VI summarizes the paper.

II. Background and Related work

A. Background

The extremely-long communication delay and time-varying topology of IPN necessitate the adoption of the "store-carry-forward (SCF)" scheme, originally designed for delay tolerant networking (DTN), to realize IP-DTs [42]. Specifically, instead of first determining the end-to-end routing path for a bundle and then forwarding it hop-by-hop accordingly, we need to temporarily store the bundle at each intermediate node until a suitable contact happens, allowing the bundle to be sent out in a "greedy" manner in hopes of reaching its destination. Although DTN has found numerous applications in networks on/around Earth, its application in IPN is fundamentally different due to the unique characteristics of IPN [43]. Therefore, it is pertinent to investigate routing and data scheduling of IP-DTs specifically, which has spurred recent studies on the topic [35–39]. In addition to theoretical approaches, the Jet Propulsion Laboratory (JPL) has developed and opensourced the interplanetary overlay network (ION) project [44, 45], providing a software platform for simulating and validating bundle-based protocols and algorithms for IPN.

B. Related Work

Although there have been algorithms designed for routing and data scheduling in Earth-based DTNs [46], they cannot be directly applied to IPN because they normally assume that contacts between nodes are random and they execute routing and data scheduling schemes based on delivery likelihood, and thus cannot perform optimization according to the contact plan of an IPN. NASA pioneered research on the routing and data scheduling of IP-DTs, and proposed the CGR algorithm [30] that plans the routing of IP-DTs based on contact plan of IPN. However, CGR ignores the queuing delay that each bundle experiences in IPN and assumes that the bundle can certainly be sent out within planned contacts, which, however, is not the case when its queuing delay can make it miss its transmission opportunity during planned contacts. This issue has motivated the studies in [31–35], which extended CGR to optimize the routing schemes of IP-DTs in consideration of the queuing of bundles in IPN nodes. Nevertheless, they all assumed that bundles are buffered in FIFO queues, omitting bundle-level scheduling. The bundle-level scheduling was optimized jointly with the routing of IP-DTs in [36–39] recently, but as we have explained in the previous section, these proposals failed to address or leverage the heterogeneity of IPN.

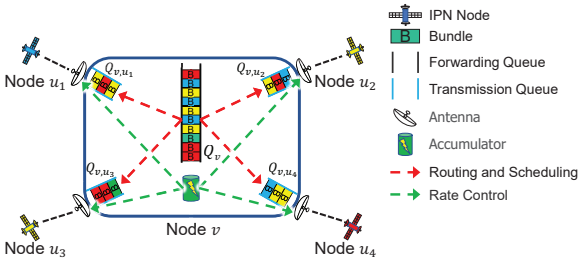

Fig. 2. Theoretical model of an IPN node.

The performance of routing and data scheduling of IP-DTs can be further improved by considering the heterogeneity of IPN. For example, the heterogenous links and nodes in IPN can be explored for controlling the data-rate of each link adaptively [35, 47, 48]. Although the feasibility of controlling the data-rates of connections in IPN based on the considerations of node storage [35, 47] and energy usage [48] has been verified, how to integrate the adaptive rate control with the routing and data scheduling of IP-DTs remains unexplored. Lyapunov optimization [41] can be leveraged to tackle such network control and resource optimization problems and has verified its effectiveness in networks on/around Earth [49], which are significantly different from IPN.

The heterogeneity of links in IPN also makes it possible to have limited state information exchange between certain nearby nodes. In [32], the mechanism of limited information exchange was explored, and the authors integrated queue information and interruptions in messages on "earliest transmission opportunity (ETO)" and shared the ETO messages among IPN nodes for better routing decision. However, they disseminated ETO messages using the flooding scheme, which led to excessive bandwidth overheads. Dhara *et al.* [40] proposed CGR-SPI, which was an enhanced CGR algorithm, to optimize routing decisions by sharing queue information among nearby nodes, but they also did not optimize the information exchange mechanism. Moreover, these studies only leveraged limited state information exchange for optimizing the routing of IP-DTs, but did not consider how to use it to enhance the performance of routing and data scheduling jointly.

III. Joint Optimization of Routing, Scheduling and Rate Control of IP-DTs

This section first describes the network model, followed by the formulation to jointly optimize the routing, scheduling and rate control of IP-DTs in an IPN node. Then, we propose an algorithm based on Lyapunov optimization to solve the problem. Table I summarizes the notations used in this section.

A. Network Model

The topology of an IPN can be conceptualized as a graph with time-varying links $G^t(V, E^t)$, with V as the node set and E^t denoting the set of temporal links. Each temporal link $e^t \in E^t$ corresponds to a contact and is a tuple $e^t(u, v, t^s, t^e, r, \tau)$, where u and v are the end nodes, t^s and t^e represent the start and end time, r indicates the highest-achievable data-rate, and τ signifies the transmission delay of the contact.

TABLE I
Major Notations Used in Problem Formulation

Notation	Description
V	the set of IPN nodes
E^t	the set of temporal links
e^t	a temporal link
u, v	the end nodes of a temporal link
B	a bundle for IP-DT
s, d	the source and destination of a bundle
β	the data size of a bundle
$\mathcal{Q}_v$	the forwarding queue on node v
$\mathcal{Q}_{v,u_i}/\mathcal{Q}_i$	the queue on node v for bundles to its i-th neighbor u_i
$\mathcal{T}$	the set of normalized time slots
$b_i(t)$	the number of bundles sent over (v, u_i) at TS t
$R_i(t)$	the number of bundles enqueued $\mathcal{Q}_i$ at TS t
W	the channel bandwidth
α	the ratio of actual data-rate to channel capacity
$\gamma_i(t)$	the ratio of channel gain to noise of (v, u_i) at TS t
$r_i(t)$	the data-rate of (v, u_i) at TS t
$\varepsilon_i(t)$	the energy consumption of (v, u_i) at TS t
$r_{i,\max}$	the maximum data-rate of (v, u_i)
$P_{v,\text{mean}}$	the budget on average power usage of node v
$Z_v(t)$	the length of virtual queue Z_v of node v at TS t
$x_{B,i}(t)$	the boolean variable for enqueuing B in $\mathcal{Q}_i$ at TS t

To address the heterogeneity of the IPN, we partition the IPN into several domains $\{\mathcal{H}_j\}$ based on the celestial bodies. Each domain $\mathcal{H}_j$ includes all the IPN nodes that are on/around a central celestial body (*i.e.*, the j-th celestial body in the IPN). We assume that the number of domains is h, and thus $V = \mathcal{H}_1 \cup \mathcal{H}_2 \cup \ldots \cup \mathcal{H}_h$. Hence, the links can be classified as intra-domain and inter-domain ones, where intra-domain links are normally much shorter than inter-domain ones. A bundle for IP-DT is modeled as $B(s, d, \beta, t^a, t^d, q)$, with s and d as its source and destination, respectively, β as its data size, t^a as its generation time at s, t^d as the deadline before when it should reach d, and q as its priority. Bundles with higher priorities will be forwarded earlier, ensuring that time-sensitive data are transmitted as quickly as possible.

B. Problem Description

We first introduce the basic theoretical model and main procedure of determining routing, scheduling and rate control for an IPN. Fig. 2 explains the theoretical model that we design for optimizing the routing, scheduling and rate control of IP-DTs in an IPN node. Note that, an IPN node can be equipped with multiple antennas to communicate with different nodes. Therefore, for each node v, we first assign a forwarding queue $\mathcal{Q}_v$ to buffer all the pending bundles that are either received from other nodes or generated locally, and then allocate a transmission queue $\mathcal{Q}_{v,u_i}$ that will store all the bundles scheduled to use the i-th neighbor node of v (*i.e.*, u_i) as its next hop. More specifically, after determining the routing and data scheduling schemes of pending bundles in $\mathcal{Q}_v$, we will move bundles from $\mathcal{Q}_v$ to $\{\mathcal{Q}_{v,u_i}\}$ accordingly. Then, when the contact of link (v, u_i) starts, our rate control determines the data-rate for sending the bundles in $\mathcal{Q}_{v,u_i}$ out according to the scheduled order, under a preset power

budget. It is easy to verify that all the three aspects (*i.e.*, the routing decision for each bundle, the bundle-level scheduling in each transmission queue, and the data-rates selected for each contact of an outgoing link) affect the IP-DT performance of an IPN node, justifying the necessity of joint optimization.

To facilitate bundle-level scheduling in each IPN node, we assume that the node is a discrete-time system operating on time slots (TS'), each of which has a fixed duration of Δt. Then, the system time is denoted as $\{\Delta t, 2\Delta t, \ldots\}$, which can then be normalized as $t \in \mathcal{T} = \{1, 2, \ldots, T\}$ for simplicity [37]. In such a discrete-time system, there are mainly two sets of constraints to address for bundle-level scheduling, *i.e.*, the energy consumption and queue stability constraints.

1) Energy Consumption Constraints: We assume that IPN node v has K antennas, each corresponding to a neighbor node u_i. Then, the rate control needs to determine the data-rate r_B used to send each bundle B in $\mathcal{Q}_{v,u_i}$ out. Since each contact should have the highest-achievable data-rate $r_{i,\max}$, determined by its physical condition, the selected data-rate r_B follows

$$0 \leq r_B \leq r_{i,\max}, \quad \forall B \in \mathcal{Q}_{v,u_i}. \tag{1}$$

With r_B selected for each bundle B, we can obtain the energy usage $\varepsilon_i(t)$ of corresponding antenna in each TS t. Since the energy available to each IPN node v is usually limited [28], we assume an upper limit on its long-term average power usage

$$\lim_{T\to\infty} \left\{ \frac{1}{T} \sum_{t=1}^{T} \mathbb{E}\left[\sum_{i=1}^{K} \varepsilon_i(t) \right] \right\} \leq P_{v,\text{mean}}. \tag{2}$$

We denote the energy consumption per unit data transfer as $\mathcal{E}(\epsilon)$, where $\epsilon = \frac{1}{r_B}$ is the transmission time per unit data for bundle B. Then, based on the studies in [50, 51], we can easily verify that $\mathcal{E}(\epsilon)$ exhibits the following characteristics:

Theorem 1. *(1) $\mathcal{E}(\epsilon) \geq 0$, (2) $\mathcal{E}(\epsilon)$ decreases monotonically with ϵ, and (3) $\mathcal{E}(\epsilon)$ is a strictly convex function of ϵ.*

We perform the following analysis based on the assumption of optimal channel coding [52] under the additive white Gaussian noise (AWGN) channel model. Note that, the channel condition and coding method are just chosen to simplify the subsequent derivations, while the general procedure and consequent algorithm design are applicable as long as *Theorem* 1 holds no matter which channel condition and coding method are used. The channel capacity can be obtained as

$$C = W \cdot \log_2 \left(1 + p_B \cdot \gamma_i(t)\right), \tag{3}$$

where W is the channel bandwidth, p_B is the antenna power used to transmit bundle B, and $\gamma_i(t)$ is the state of the channel at TS t, defined as the ratio of channel gain to channel noise[1]. Then, the data-rate used for transmitting bundle B can be denoted as $r_B = \alpha \cdot C,\ \alpha \in (0, 1)$, and thus

$$\begin{aligned} \mathcal{E}(\epsilon) &= \frac{1}{r_B} \cdot p_B = \frac{1}{r_B} \cdot \left\{ \left[2^{\left(\frac{r_B}{\alpha \cdot W}\right)} - 1 \right] \cdot \frac{1}{\gamma_i(t)} \right\} \\ &= \frac{\epsilon}{\gamma_i(t)} \cdot \left[2^{\left(\frac{1}{\epsilon \cdot \alpha \cdot W}\right)} - 1 \right]. \end{aligned} \tag{4}$$

We can easily verify that $\mathcal{E}(\epsilon)$ in Eq. (4) satisfies *Theorem* 1.

[1]Note that, this work considers time-varying channel state, *i.e.*, the communication over a channel can be degraded or even interrupted due to unpredicted reasons such as deep space EM interference, *etc*, but for simplicity, we assume that the state of each channel stays constant within a TS.

2) Queue Stability Constraints: As explained above, the routing decisions made by node v on bundles affect the enqueue rate $R_i(t)$ of each transmission queue $\mathcal{Q}_{v,u_i}$. For the clarity, we abbreviate $\mathcal{Q}_{v,u_i}$ as $\mathcal{Q}_i$ and use $\mathcal{Q}_i(t)$ to denote the queue length of $\mathcal{Q}_{v,u_i}$ at TS t in the following derivations. Then, the update of the queue state of $\mathcal{Q}_i$ can be expressed as

$$\mathcal{Q}_i(t+1) = \max\left[\mathcal{Q}_i(t) - b_i(t), 0\right] + R_i(t), \tag{5}$$

where $b_i(t)$ is the number of bundles sent over (v, u_i) at TS t and it depends on the rate control decisions of node v. Meanwhile, none of the transmission queues grow indefinitely. Hence, $\mathcal{Q}_i$ must satisfy the following condition

$$\lim_{t\to\infty} \frac{\mathbb{E}\left[\mathcal{Q}_i(t)\right]}{t} = 0. \tag{6}$$

The objective of the joint optimization of the routing, scheduling and rate control of IP-DTs is to minimize the long-term average queuing delay and the cost due to bundle losses at each IPN node v. However, by checking Eqs. (2) and (5), we find that the routing, scheduling and rate control of IP-DTs at a TS jointly affect the queue status and energy usage of node v at future TS', which leads to a fairly complex optimization.

C. Lyapunov-based Optimization Model

In order to solve the aforementioned optimization, we leverage the theory of Lyapunov optimization [41], which is commonly used in queue optimization problems and can achieve relatively good performance. The Lyapunov-based optimization model is built as follows.

We first define a virtual queue Z_v for each IPN node v. Let $Z_v(t)$ represent the queue length of Z_v at TS t, with the initial condition $Z_v(0) = 0$. And the update formula for $Z_v(t)$ is

$$Z_v(t+1) = \max\left[\left(Z_v(t) + \sum_{i=1}^{K} \varepsilon_i(t) - P_{v,\text{mean}} \cdot \Delta t \right), 0 \right]. \tag{7}$$

Here, $Z_v(t)$ can be interpreted as the "energy liability", *i.e.*, as long as $Z_v(t)$ satisfies the queue stable condition in Eq. (6), the energy constraint in Eq. (2) is satisfied [41]. We proceed to optimize the operations on all queues in node v, *i.e.*, the transmission queue set $\mathbf{Q}(t) \triangleq (\mathcal{Q}_1(t), \mathcal{Q}_2(t), \ldots, \mathcal{Q}_K(t))$ and the virtual queue $Z_v(t)$, resulting in an overall queue set as $\Theta(t) = (\mathbf{Q}(t), Z_v(t))$, with Lyapunov function defined as

$$L\left(\Theta(t)\right) \triangleq \frac{1}{2}\left[\sum_{i=1}^{K} \mathcal{Q}_i^2(t) + Z_v^2(t) \right]. \tag{8}$$

Then, the conditional Lyapunov drift can be defined as

$$\Delta\left(\Theta(t)\right) \triangleq \mathbb{E}\left[L\left(\Theta(t+1)\right) - L\left(\Theta(t)\right) | \Theta(t) \right]. \tag{9}$$

Next, we use Lyapunov drift $\Delta\left(\Theta(t)\right)$ to continuously drive the Lyapunov function in Eq. (8) towards low congestion

$$\begin{aligned} &\Delta\left(\Theta(t)\right) = \mathbb{E}\left[L\left(\Theta(t+1)\right) - L\left(\Theta(t)\right) | \Theta(t) \right] \\ =&\mathbb{E}\left\{ \frac{1}{2}\left[\sum_{i=1}^{K} \mathcal{Q}_i^2(t+1) - \sum_{i=1}^{K} \mathcal{Q}_i^2(t) + Z_v^2(t+1) - Z_v^2(t) \right] | \Theta(t) \right\} \\ \leq& M + \mathbb{E}\left[\sum_{i=1}^{K} \mathcal{Q}_i(t) \cdot R_i(t) | \Theta(t) \right] - \mathbb{E}\left[\sum_{i=1}^{K} \mathcal{Q}_i(t) \cdot b_i(t) | \Theta(t) \right] \\ &+ \mathbb{E}\left[Z_v(t) \left(\sum_{i=1}^{K} \varepsilon_i(t) - P_{v,\text{mean}} \cdot \Delta t \right) | \Theta(t) \right], \end{aligned} \tag{10}$$

where M is the upper bound,

$$M \triangleq \max\left\{ \mathbb{E}\left[\sum_{i=1}^{K}\left(\frac{R_i^2(t)+b_i^2(t)}{2}\right)|\Theta(t)\right] + \mathbb{E}\left[\frac{\left(\sum_{i=1}^{K}\varepsilon_i(t)-P_{v,\text{mean}}\cdot\Delta t\right)^2}{2}|\Theta(t)\right]\right\}. \tag{11}$$

To get Eq. (10), we use the inequality ($\mathcal{Q}\geq 0$, $b\geq 0$, $R\geq 0$):

$$\{\max[\mathcal{Q}-b,0]+R\}^2 \leq \mathcal{Q}^2+R^2+b^2+2\mathcal{Q}\cdot(R-b). \tag{12}$$

We can reduce the average queue backlog by minimizing the upper bound of the Lyapunov drift in Eq. (10), and ensure that all the queues in $\Theta(t)$ are strongly stable [37, 41]. We also incorporate a penalty term to the objective function to further evaluate the long-term performance of routing decisions, aiming to minimize the "drift plus penalty" [41]. Hence, the optimization objective is

$$\begin{aligned}\text{Minimize}\quad F(t) &= \sum_{i=1}^{K}\mathcal{Q}_i(t)\cdot R_i(t)-\sum_{i=1}^{K}\mathcal{Q}_i(t)\cdot b_i(t)\\ &+ Z_v(t)\left(\sum_{i=1}^{K}\varepsilon_i(t)-P_{v,\text{mean}}\cdot\Delta t\right)+\lambda\cdot\mathcal{P}(t),\end{aligned} \tag{13}$$

where $\mathcal{P}(t)$ is the penalty term and λ is its weight, which is typically chosen empirically, *i.e.*, the term $\lambda\cdot\mathcal{P}(t)$ reflects the tradeoff between queue backlog and routing decisions. Specifically, we can formulate $\mathcal{P}(t)$ as

$$\mathcal{P}(t) = -\sum_{i=1}^{K}\sum_{B\in\mathcal{Q}_v} w_{B,i}(t)\cdot x_{B,i}(t), \tag{14}$$

where $w_{B,i}(t)$ is the normalized performance gain achieved by selecting node u_i as the next hop of bundle B at TS t, and $x_{B,i}(t)$ is the boolean variable that equals 1 if bundle B is enqueued in $\mathcal{Q}_i$ at TS t, and 0 otherwise. According to our previous study [39], $w_{B,i}(t)$ can be empirically formulated as the weighted sum of factors such as the projected delivery time, path length, and queue lengths of subsequent nodes on the path (if state information exchange is enabled).

We then rewrite the objective function $F(t)$ in Eq. (13) to have two terms as

$$\begin{aligned}F(t) &= \left[\sum_{i=1}^{K}\mathcal{Q}_i(t)\cdot R_i(t)+\lambda\cdot\mathcal{P}(t)\right]\\ &-\left[\sum_{i=1}^{K}\mathcal{Q}_i(t)\cdot b_i(t)-Z_v(t)\left(\sum_{i=1}^{K}\varepsilon_i(t)-P_{v,\text{mean}}\cdot\Delta t\right)\right],\end{aligned} \tag{15}$$

and decompose the optimization into two subproblems, namely, the routing and scheduling and the rate control subproblems related to the first and second terms in Eq. (15), respectively.

1) Routing and Scheduling Subproblem: With Eqs. (13)-(15), we formulate the routing and scheduling subproblem as

$$\begin{aligned}\text{Maximize}\ F_1(t) &= \lambda\sum_{i=1}^{K}\sum_{B\in\mathcal{Q}_v} w_{B,i}(t)x_{B,i}(t)-\sum_{i=1}^{K}\mathcal{Q}_i(t)R_i(t)\\ s.t.\ &\sum_{B\in\mathcal{Q}_v} x_{B,i}(t)=R_i(t),\quad \forall i\in[1,K],\ \forall t\in\mathcal{T},\\ &\sum_{i=1}^{K} x_{B,i}(t)\leq 1,\quad \forall B\in\mathcal{Q}_v,\ \forall t\in\mathcal{T},\end{aligned} \tag{16}$$

where the first constraint reveals the relation between $R_i(t)$ and $x_{B,i}(t)$, and the second constraint ensures that we only assign at most one next hop to each bundle. Then, the objective function in Eq. (16) can be further transformed into

$$\begin{aligned}F_1(t) =&\lambda\sum_{i=1}^{K}\sum_{B\in\mathcal{Q}_v} w_{B,i}(t)x_{B,i}(t)-\sum_{i=1}^{K}\left[\mathcal{Q}_i(t)\sum_{B\in\mathcal{Q}_v} x_{B,i}(t)\right]\\ =&\sum_{i=1}^{K}\sum_{B\in\mathcal{Q}_v}\left[\lambda\cdot w_{B,i}(t)-\mathcal{Q}_i(t)\right]\cdot x_{B,i}(t),\end{aligned} \tag{17}$$

which leads to a straightforward strategy for deciding the value of each $x_{B,i}(t)$, *i.e.*, for each bundle B, we find the values of $\{x_{B,i}(t)\}$ that can maximize $\lambda\cdot w_{B,i}(t)-\mathcal{Q}_i(t)$ as

$$x_{B,i}(t)^* = \underset{x_{B,i}(t)}{\text{argmax}}\left[\lambda\cdot w_{B,i}(t)-\mathcal{Q}_i(t)\right],\quad \forall B\in\mathcal{Q}_v. \tag{18}$$

2) Rate Control Subproblem: With Eqs. (13) and (15), we formulate the rate control subproblem as

$$\begin{aligned}\text{Maximize}\quad F_2(t) &= \sum_{i=1}^{K}\mathcal{Q}_i(t)b_i(t)\\ &- Z_v(t)\left[\sum_{i=1}^{K}\varepsilon_i(t)-P_{v,\text{mean}}\cdot\Delta t\right].\end{aligned} \tag{19}$$

To represent the impact of rate control decisions on the IPN node, we can express $b_i(t)$ and $\varepsilon_i(t)$ as:

$$\begin{cases} b_i(t) = b_i(\vec{r}_B(t),\mathbf{S}(t)),\\ \varepsilon_i(t) = \sum_{B\in\mathcal{B}_i(t)}\beta_B\cdot\mathcal{E}\left(\frac{1}{r_B}\right),\end{cases} \tag{20}$$

where $\mathcal{B}_i(t)$ is the set of the bundles in $\mathcal{Q}_i$ transmitted at TS t, $\vec{r}_{i,B}(t)$ is the rate control vector for transmitting bundle in TS t (*i.e.*, $\vec{r}_{i,B}(t)=\{r_B|B\in\mathcal{B}_i(t)\}$), and $\mathbf{S}(t)$ is the current state vector of node v and (v,u_i) (*i.e.*, $\mathbf{S}(t)=\{\mathbf{Q}(t),Z_v(t),\gamma_i(t),(t^s,t^e,r,\tau)\}$).

In order to clarify the relation between $\vec{r}_{i,B}(t)$ and $b_i(t)$, we introduce the following theorem.

Theorem 2. *As for $\mathcal{B}_i(t)$, the most energy-efficient rate control strategy satisfies $r_{B_l}=r_{B_m},\ \forall B_l,B_m\in\mathcal{B}_i(t)$.*

Proof: We first check the simplest case with two bundles $\mathcal{B}_i(t)=\{B_1,B_2\}$, and there are only two strategies to test:

- We have $r_{B_1}<r_{B_2}$ (or the other way around), and thus the transmission latencies are $l_{B_1}=\frac{\beta_{B_1}}{r_{B_1}}$ and $l_{B_2}=\frac{\beta_{B_2}}{r_{B_2}}$, with $l_{B_1}+l_{B_2}=\Delta t$.
- We have $r^*_{B_1}=r^*_{B_2}=r^*$, where $r^*=\frac{\beta_{B_1}+\beta_{B_2}}{\Delta t}$.

Here, β_{B_1} is the data size of bundle B_1 and likewise β_{B_2}. The energy consumptions of the two strategies are $\varepsilon_i(r_{B_1}, r_{B_2})$ and $\varepsilon_i(r^*_{B_1}, r^*_{B_2})$, respectively. Then, we can prove

$$\begin{aligned}
&\varepsilon_i(r_{B_1}, r_{B_2}) - \varepsilon_i(r^*_{B_1}, r^*_{B_2}) \\
=&\beta_{B_1}\mathcal{E}\left(\frac{l_{B_1}}{\beta_{B_1}}\right) + \beta_{B_2}\mathcal{E}\left(\frac{l_{B_2}}{\beta_{B_2}}\right) - (\beta_{B_1}+\beta_{B_2})\mathcal{E}\left(\frac{1}{r^*}\right) \\
=&\beta_{B_1}\mathcal{E}\left(\frac{l_{B_1}}{\beta_{B_1}}\right) + \beta_{B_2}\mathcal{E}\left(\frac{l_{B_2}}{\beta_{B_2}}\right) - (\beta_{B_1}+\beta_{B_2})\mathcal{E}\left(\frac{l_{B_1}+l_{B_2}}{\beta_{B_1}+\beta_{B_2}}\right) \\
>&0,
\end{aligned} \tag{21}$$

by leveraging the convex nature of $\mathcal{E}(\cdot)$ (*i.e.*, *Theorem* 1). This proof can be easily generalized to the case with an arbitrary number of bundles, and thus we prove *Theorem* 2. ■

Hence, the rate control decisions $\vec{r}_{i,B}(t)$ for bundles transmitted at TS t can be simplified to determine $r_i(t)$ at TS t under the following constraints[2]

$$0 \le r_i(t) \le r_{i,\max}, \quad \forall i \in [1, K],\ \forall t \in \mathcal{T}. \tag{22}$$

We assume that each TS t is either included in or excluded from a contact completely, define the average size of the bundles for being sent over (v, u_i) at TS t as $\bar{\beta}$, and get

$$\begin{cases} b_i(t) = \dfrac{\Delta t \cdot r_i(t)}{\bar{\beta}}, \\ \varepsilon_i(t) = \Delta t \cdot r_i(t) \cdot \mathcal{E}\left(\dfrac{1}{r_i(t)}\right) = \dfrac{\Delta t}{\gamma_i(t)}\left[2^{\frac{r_i(t)}{\alpha \cdot W}} - 1\right], \end{cases} \tag{23}$$

Note that, the term $Z_v(t)P_{v,\text{mean}} \cdot \Delta t$ in Eq. (19) is a constant, and thus by removing it and substituting Eq. (23) in Eq. (19), we transform the objective function into

$$\begin{aligned}
\text{Maximize} \quad F_2(t) =& \sum_{i=1}^{K} \mathcal{Q}_i(t) \cdot \left[\frac{\Delta t \cdot r_i(t)}{\bar{\beta}}\right] \\
&- Z_v(t) \sum_{i=1}^{K} \left[\frac{\Delta t}{\gamma_i(t)}\right] \cdot \left(2^{\frac{r_i(t)}{\alpha W}} - 1\right).
\end{aligned} \tag{24}$$

In order to maximize the $F_2(t)$ in Eq. (24), we obtain its partial derivative with respect to $r_i(t)$ as

$$\frac{\partial F_2(t)}{\partial r_i(t)} = \mathcal{Q}_i(t)\left[\frac{\Delta t}{\bar{\beta}}\right] - Z_v(t)\left[\frac{\Delta t}{\gamma_i(t)}\right]\left[2^{\frac{r_i(t)}{\alpha W}}\left(\frac{\ln(2)}{\alpha W}\right)\right], \tag{25}$$

find the zeros of the equation by solving

$$\mathcal{Q}_i(t)\left[\frac{\Delta t}{\bar{\beta}}\right] - Z_v(t)\left[\frac{\Delta t}{\gamma_i(t)}\right]\left[2^{\frac{r_i(t)}{\alpha W}}\left(\frac{\ln(2)}{\alpha W}\right)\right] = 0, \tag{26}$$

and get

$$\tilde{r}_i(t) = \alpha \cdot W \cdot \log_2\left[\frac{\alpha \cdot W \cdot \mathcal{Q}_i(t) \cdot \gamma_i(t)}{\ln(2) \cdot Z_v(t) \cdot \bar{\beta}}\right]. \tag{27}$$

As $\frac{\partial^2 F_2(t)}{\partial r_i^2(t)} \le 0$ always holds, we get the optimal rate $r_i^*(t)$ by incorporating the constraint in Eq. (22):

$$r_i^*(t) = \begin{cases} \tilde{r}_i(t), & \text{if } 0 < \tilde{r}_i(t) < r_{i,\max}, \\ r_{i,\max}, & \text{if } \tilde{r}_i(t) \ge r_{i,\max}, \\ 0, & \text{if } \tilde{r}_i(t) \le 0. \end{cases} \tag{28}$$

Algorithm 1: L-RSRC Algorithm

$t = 0$, $Z_v(t) = 0$ and initialize $\mathcal{Q}_v$ and $\{\mathcal{Q}_i\}$;
while *the IPN node* $v \in V$ *is operational* **do**
  insert all the newly generated/received bundles in $\mathcal{Q}_v$;
  for *each bundle* $B \in \mathcal{Q}_v$ **do**
    calculate N paths for B whose projected delivery time is the earliest, and compute $w_{B,i}(t)$;
    if *at least one path is found* **then**
      select the next hop for B with Eq. (18);
      move B to the corresponding queue $\mathcal{Q}_i$;
    else
      keep B in $\mathcal{Q}_v$;
    end
  end
  for *each queue* $\mathcal{Q}_i$ **do**
    if (v, u_i) *is in contact* **then**
      obtain $\bar{\beta}$ for bundles in $\mathcal{Q}_i$, and calculate $r_i^*(t)$ with Eq. (28);
    else
      $r_i(t) = 0$;
    end
    adjust the order of bundles in $\mathcal{Q}_i$ with the data scheduling algorithm in [39];
  end
  calculate $\varepsilon_i(t)$ and update $Z_v(t)$ with Eq. (7);
  for *each queue* $\mathcal{Q}_i$ **do**
    if (v, u_i) *is in contact* **then**
      transmit bundles in $\mathcal{Q}_i$ in sequence;
    end
  end
  $t = t + 1$, remove expired bundles in $\mathcal{Q}_v$;
end

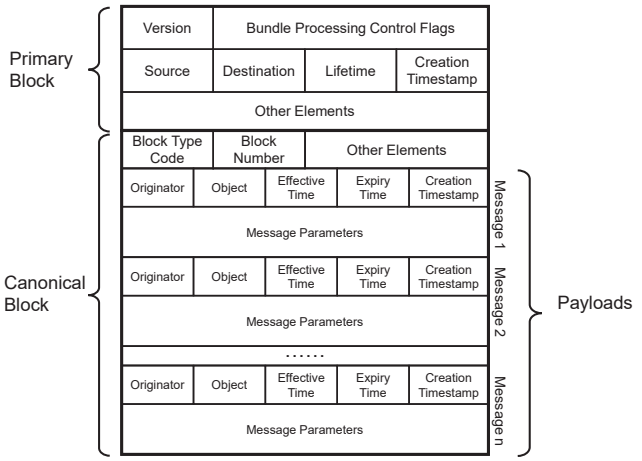

Fig. 3. Bundle format for encapsulating state information.

D. Algorithm Description

Based on the above derivations, we design a distributed routing, scheduling and rate control algorithm based on Lyapunov optimization (L-RSRC), as shown in *Algorithm* 1.

Line 1 initializes the process. Then, if an IPN node v is operational, the while-loop of *Lines* 2-28 performs the joint optimization of routing, scheduling and rate control of IP-DTs in discrete time. Specifically, the operations at each TS are explained as follows. First, after updating the forwarding queue $\mathcal{Q}_v$ to enqueue all the newly generated/received bundles (*Line* 3), the for-loop of *Lines* 4-12 determines the routing of each bundle in $\mathcal{Q}_v$ by selecting a proper next hop for it using Eq. (18). *Line* 5 calculates routing paths for bundle B using the CGR algorithm [30], based on the scheduled contacts between IPN nodes. Next, bundles with designated next hops are enqueued to corresponding transmission queues, and the for-loop of *Lines* 13-20 checks each queue $\mathcal{Q}_i$ to accomplish the rate control of each bundle there, using Eq. (28). Note that $\mathcal{Q}_i(t)$ is constant after each TS t with all the enqueued bundles transmitted. After determining the transmission data-rate of each bundle, we leverage our data scheduling algorithm in [39] to adjust the transmission order of the bundles in $\mathcal{Q}_i$ (*Line* 19), and the algorithm can adjust the order of bundles in $\mathcal{Q}_i$ by jointly considering their attributes of sizes, priorities, time-to-lives (TTLs), *etc.*, to get the minimum expected queuing delay. *Line* 21 calculates $\varepsilon_i(t)$ and updates the virtual queue $Z_v(t)$. Finally, the actual transmission of bundles is executed according to the established scheme (*Lines* 23-25).

Complexity Analysis: *Algorithm* 1 runs independently on each IPN node and its time complexity can be analyzed as follows. The complexity of calculating N paths in *Line* 5 is $O\left(N \cdot |C| \cdot \log(|C|)\right)$, where $|C|$ is the size of the contact plan [53], while the complexity of $w_{B,i}(t)$ calculation and routing decision is $O(K)$. Hence, the complexity of the routing phase is $O\left(|\mathcal{Q}_v| \cdot (N \cdot |C| \cdot \log(|C|) + K)\right)$. The complexity for getting $r_i^*(t)$ is $O(1)$, and thus the complexity of the rate control phase is $O(K)$. The complexity of the data scheduling in *Line* 19 is $O(K^2 \cdot (|\mathcal{Q}_v|^2 + \frac{r_i(t)}{\beta}))$ according to the analysis in our previous work [39]. Finally, the overall complexity of *Algorithm* 1 is $O\left(|\mathcal{Q}_v|N|C|\log(|C|) + K^3\left(|\mathcal{Q}_v|^2 + \frac{r_i(t)}{\beta}\right)\right)$.

IV. Limited State Information Exchange

The L-RSRC algorithm proposed in the previous section needs to evaluate routing paths and channel states to reach a proper decision. If we run the algorithm in a purely-distributed manner, each IPN node relies solely on its local information to make IP-DT decisions, which can be suboptimal given the limited information available to each node individually. Therefore, in this section, we leverage the heterogeneity of IPN to design a limited state information exchange mechanism that enables IPN nodes make more informed decisions for IP-DTs, especially to cope with unexpected link interruptions and sudden surges in traffic.

A. Bundle Encapsulation and Message Format

If two IPN nodes are close or can communicate with short latency, they can engage in state information exchange, while the actual threshold on distance or communication latency can be set empirically. We encapsulate the state information of a node in a bundle intended for state messages. The format of the state message is designed based on that has been standardized in the bundle protocol [54]. As shown in Fig. 3, the primary block (*i.e.*, the bundle header) contains the necessary control information for processing the bundle, such as the bundle protocol version, source and destination, *etc*. Here, we leverage one unused bit in the *Bundle Processing Control Flags* field to identify whether a bundle is for a state message. Specifically, the flag bit is named as *Flag_Info*, which is set as 1 for a state message bundle, and 0 otherwise. If an IPN node sees a state message bundle, it assigns the highest priority to the bundle to ensure the timeliness of delivery. Following the primary block, we have the canonical block [54], which contains the payloads that encapsulate the state information.

The canonical block contains a series of payloads, *i.e.*, the application data units (ADUs), each of which is characterized by the fields about its originator (n_{ori}) (*i.e.*, the IPN node that generates it), associated object (e_{obj}) (*i.e.*, a transmission queue and its outgoing link), effective time length (t_{eff}), expiry time (t_{exp}) and creation timestamp (t_{c}). Next, the section of message parameters encodes the state information for exchange, which is mainly about each transmission queue in a node, including the queue length, total buffered data size, earliest transmission opportunity (ETO) [32], data-rate and health of the queue's outgoing link, *etc*. The state information can be used to update $\{w_{B,i}(t)\}$ to $\{w'_{B,i}(t)\}$ as follows, ensuring that the penalty obtained by substituting $\{w'_{B,i}(t)\}$ into Eq. (14) accurately reflects the status of subsequent nodes along a bundle's routing path:

$$w'_{B,i}(t) = w_{B,i}(t) - \eta \sum_{u \in \mathbf{P}_i} \theta^{hop} \cdot \Psi_v^u, \tag{29}$$

where η is the modification factor, θ^{hop} is the discount factor of node u based on the hop-count, hop, from u to v on path $\mathbf{P}_i$, and Ψ_v^u is the evaluation value determined by node v using the received state information about node u. The values of η and θ^{hop} are determined empirically.

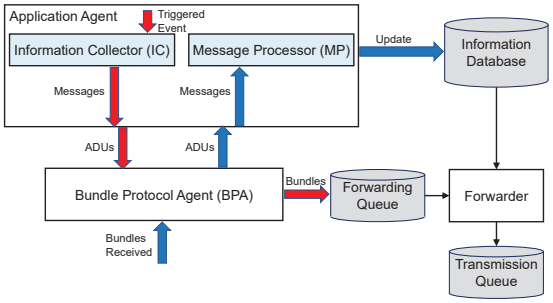

Fig. 4. Procedure of generating and processing state message bundles.

B. Generation and Processing of State Message Bundles

Fig. 4 illustrates our design for generating and processing the state message bundles in each IPN node v. Each node maintains an information database to store the state information received from its neighbors, which is used to further optimize its decisions on routing, scheduling and rate

[2]If a bundle takes multiple TS' to transmit, we can assign different data-rates across TS' by treating the segments of the bundle as multiple ones.

control of IP-DTs. We design an information collector (IC) and a message processor (MP) to be integrated into the application agent specified in [54], where the IC collects the state information about the node and generates state messages as needed, while the MP handles state messages received from neighbors and updates the information database accordingly. In addition, we enhance the bundle protocol agent (BPA) defined in [54] to support the encapsulation and parsing of state message bundles.

C. Triggering and Dissemination Mechanisms

Finally, we elaborate on the mechanisms for triggering the generation of state message bundles and disseminating them efficiently. For the triggering mechanism, it is essential to balance the tradeoff between the timeliness and accuracy of state information and the overheads associated with generating, transmitting and processing this information. We consider the following three scenarios:

- Fixed time interval based triggering (FTT): state message bundles are generated periodically.
- Queue change based triggering (QCT): state message bundles are generated when the length of a transmission queue changes beyond a preset threshold.
- Link change based triggering (LCT): state message bundles are generated when the status of a link changes unexpectedly to affect its data transmission significantly.

The dissemination mechanism decides which nodes should receive a state message, considering the message's timeliness and bandwidth overhead. To send a state message bundle to multiple destinations, we unicast it multiple times, making the bundle multicast compatible with the algorithm designed in the previous section. We consider the following three scenarios:

- TTL: A state message bundle propagates in the IPN until its preset survival time expires.
- Maximum hop count (MHC): A state message bundle is forwarded until its hop count reaches a preset upper-limit.
- Intra-domain only (IDO): A state message bundle is only forwarded within the domain of its source.

V. Performance Evaluations

In this section, we perform extensive simulations to compare our proposed L-RSRC algorithm with existing benchmarks and to explore the performance gain achieved by various state information exchange mechanisms.

A. Simulation Setup

We consider two IPN topologies, *i.e.*, IPN-1 and IPN-2, as shown in Figs. 5(a) and 5(b), respectively. Specifically, IPN-1 covers three domains associated with Earth, Moon, and Mars, respectively, and it consists of 8 nodes, including a ground control center, 3 ground stations, 2 rovers, and 2 satellites, while IPN-2 includes two more domains concerning Mercury and Venus, making 14 nodes in it, *i.e.*, a ground control center, 3 ground stations, 2 rovers, and 8 satellites. Each simulation spans 24 hours in the IPNs, where motions of IPN nodes are emulated using the Satellite Tool Kit (STK) [55]. In each node,

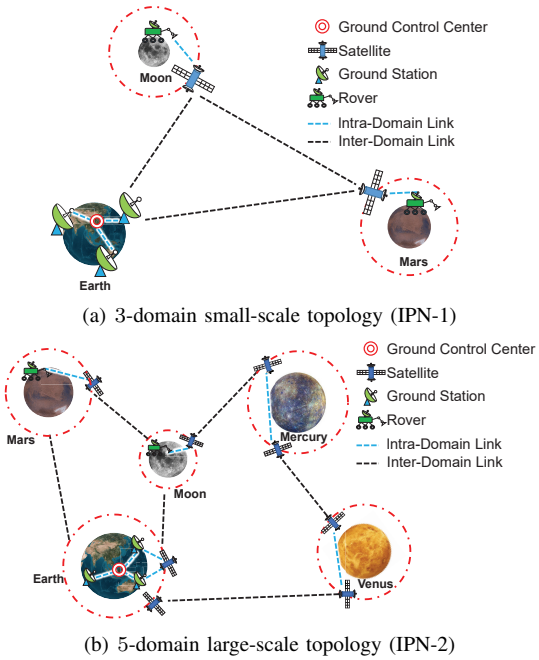

(a) 3-domain small-scale topology (IPN-1)

(b) 5-domain large-scale topology (IPN-2)

Fig. 5. IPN topologies used in simulations.

bundles are dynamically generated with Poisson traffic model. The bundles are categorized into three priorities based on their data sizes: 1) high priority (bundles carrying critical control commands or state information, ranging from 1 to 8 KBytes.), 2) medium priority (bundles used for transmitting telemetry data and operating status, ranging from 16 to 64 KBytes.) and 3) low priority (bundles used for scientific data transfer, including images and sensor readings, ranging from 128 to 1024 KBytes.). The distribution ratio of bundles in the three priorities is 1:1:18. Table II lists the simulation parameters. To ensure statistical accuracy, we average the results from 5 independent runs to get each data point in the simulations.

TABLE II
Simulation Parameters

Parameters	Values
Time span	24 hours (86, 400 seconds)
Duration of a TS Δt	1 second
Average lifetime of bundles	10, 000 seconds (IPN-1)
	20, 000 seconds (IPN-2)
W	10 MHz
α	0.9
$\gamma_i(t)$	$[0.003, 0.01]$
$P_{v,\text{mean}}$	$[0.5, 5.0]$ KW
$r_{i,\max}$	$[50, 500]$ kbps
η	0.1
θ	0.8

Our simulations compare the proposed L-RSRC algorithm with 4 existing approaches in the literature: 1) CGR [30], 2) EAODR [34], 3) MARS[3] [36], and 4) the FD-RDS-appro that

[3]MARS [36] actually used multiple weight settings. In the following discussion, we only show the results of the one that performs the best in most of the simulation scenarios.

we proposed in [39]. As none of the benchmarks incorporates rate control of IP-DTs, we assume that they all just evenly distribute the available energy for an IPN node in each TS to all of its outgoing links that are in contact.

B. IPN without Unexpected Interruptions

We first conduct simulations for the ideal scenario where there are no unexpected interruptions in IPN, and the limited state information exchange is disabled. The results obtained in IPN-1 are shown in Fig. 6, which shows that our L-RSRC achieves the best IP-DT performance among all the algorithms, *i.e.*, the lowest average end-to-end (E2E) latency and highest delivery ratio. Specifically, on average, L-RSRC reduces E2E latency and improves delivery ratio by 43.80% and 33.21%, respectively, over the benchmarks. This superiority stems from L-RSRC considering various aspects of an IPN node to jointly optimize the routing, scheduling and rate control of IP-DTs. FD-RDS-appro also optimizes the routing and scheduling of IP-DTs jointly, and thus it follows closely in performance.

The simulations are then repeated with IPN-2, and the results are in Fig. 7, which still follow the similar trends as those in Fig. 6. To adapt to the larger topology of IPN-2, we double the average lifetime of bundles in the simulations. This is the reason why the delivery ratio in IPN-2 is higher than that in IPN-1 when the algorithm and traffic load are the same. We notice that this time, the performance gains achieved by L-RSRC over the benchmarks on delivery ratio are much larger than those in Fig. 6, with an improvement of 46.65% in E2E latency and 52.54% in delivery ratio on average over the benchmarks, respectively. This suggests that the optimization of rate control achieved by L-RSRC becomes more important in larger and more complex IPNs. It is interesting to notice that the average E2E latency from L-RSRC is slightly longer than that from FD-RDS-appro when the traffic load is higher than 1.3 bundles/minute/node. This can be understood by the larger gaps between the delivery ratios from the two algorithms at such loads, *i.e.*, L-RSRC successfully delivers many more bundles with relatively long transmission distances.

C. IPNs with Unexpected Interruptions

We then consider more practical scenarios where unexpected interruptions can happen on inter-domain links due to the extreme EM interference in deep space. Specifically, we explore two such scenarios: 1) *Scenario*-1, where each susceptible link randomly experiences $[3, 5]$ interruptions in a simulation, and the duration of each interruption is $[259, 2592]$ seconds (*i.e.*, $[0.3\%, 3\%]$ of the simulation time (24 hours)), and 2) *Scenario*-2, where each susceptible link is randomly interrupted for $[3, 8]$ times in a simulation, and the duration of each interruption is $[432, 4320]$ seconds (*i.e.*, $[0.5\%, 5\%]$ of 24 hours). This time, we assume that limited state information exchange is turned on, with the FTT mechanism, which promotes each node to generate a state message bundle every 200 seconds, and the TTL mechanism sets its survival time as $1,000$ seconds. The length of each state message bundle is assumed to be 1 KByte. Regarding the algorithms, we consider two versions of L-RSRC, *i.e.*, one with state information exchange (L-RSRC-info) and without (L-RSRC). Since CGR, EAODR, MARS and FD-RDS-appro do not consider state information exchange, we introduce a new benchmark called CGR-ETO [32], which leverages state information from other nodes to optimize IP-DTs, to replace CGR.

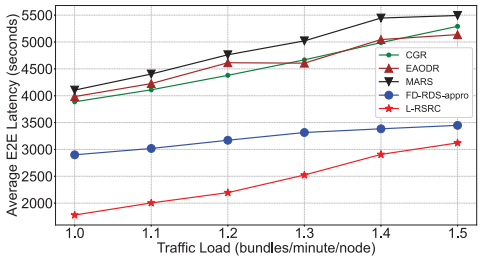

(a) Average E2E latency

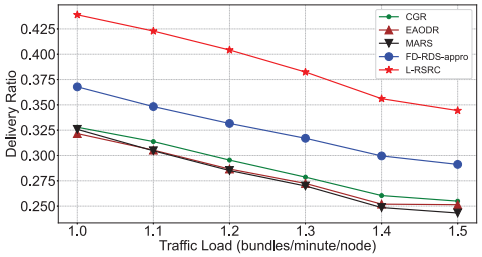

(b) Delivery ratio

Fig. 6. IPN-1 without unexpected interruptions or information exchange.

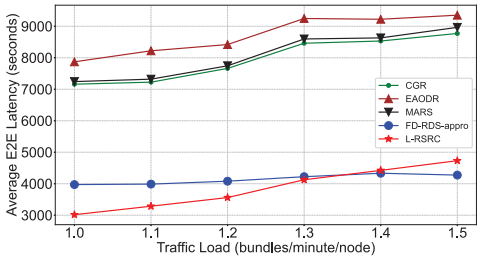

(a) Average E2E latency

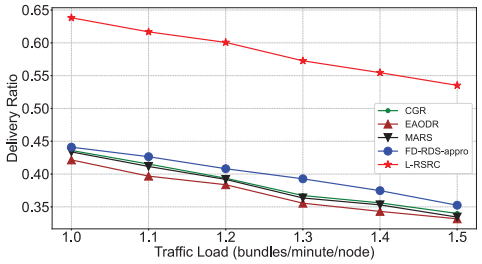

(b) Delivery ratio

Fig. 7. IPN-2 without unexpected interruptions or information exchange.

The results obtained in IPN-1 are shown in Figs. 8 and 9 for the two interruption scenarios, respectively. Unexpected interruptions indeed degrade the performance of each algorithm noticeably, when compared to their counterparts in Fig. 6. However, L-RSRC still outperforms all the benchmarks, achieving average improvements in E2E latency of 40.79% and 37.83%, and average increases in delivery ratio of 28.96% and 28.21% in the two interruption scenarios, respectively. We also observe that the inclusion of limited state information exchange can further improve the performance of L-RSRC.

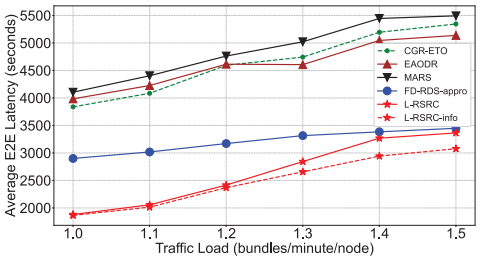

(a) Average E2E latency

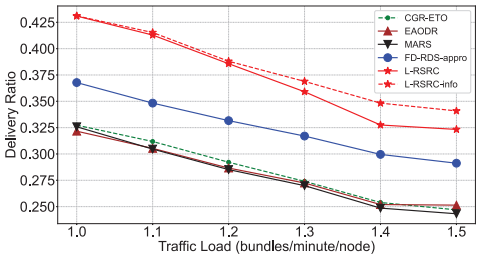

(b) Delivery ratio

Fig. 8. IPN-1 with unexpected interruptions (*Scenario*-1).

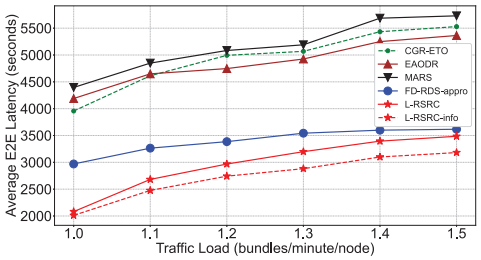

(a) Average E2E latency

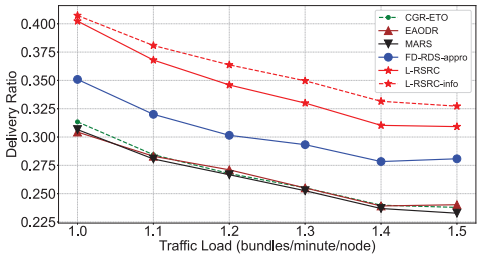

(b) Delivery ratio

Fig. 9. IPN-1 with unexpected interruptions (*Scenario*-2).

Specifically, L-RSRC-info achieves average improvements of 5.71% and 7.95% in E2E latency and average increases of 2.37% and 4.58% in delivery ratio over L-RSRC in the two scenarios, respectively. The gaps between L-RSRC-info and L-RSRC in Figs. 8 and 9 become larger when traffic load increases or there are more and severer interruptions, further justifying the value of limited state information exchange.

Figs. 10 and 11 plot the results obtained in IPN-2. L-RSRC and L-RSRC-info still outperform the benchmarks significantly in both the delivery ratio and average E2E latency, with average improvements of 45.33% and 42.57% in E2E latency and 51.41% and 50.49% in delivery ratio across the two interruption scenarios, respectively, but their average E2E latencies are similar as those from FD-RDS-appro. This verifies that our proposals can better adapt to scenarios with unexpected interruptions. As explained above, L-RSRC successfully delivers more bundles with relatively long transmission distances, making its average E2E latency slightly longer than that of FD-RDS-appro when the traffic load is high. Meanwhile, it is interesting to notice that compared with the results of IPN-1, the performance gaps between L-RSRC-info and L-RSRC become smaller, with L-RSRC-info achieving 1.92% and 5.38% reductions in E2E latency and 0.82% and 1.14% improvements in delivery ratio on average in the two interruption scenarios, respectively. This can be attributed to two factors: 1) the longer average transmission latency in IPN-2 degrades the timeliness of state information, and 2) the larger topology of IPN-2 increases the communication overheads due to state information exchange, offsetting certain performance gains. Therefore, finding the best state information exchange mechanism becomes relevant to further optimize the tradeoff between performance gains and communication overheads.

D. Comparisons of State Information Exchange Mechanisms

Finally, we compare the state information exchange mechanisms and explore their impacts on L-RSRC-info's performance. The simulations use the highest traffic load (*i.e.*, 1.5 bundles/minute/node) and interruption *Scenario*-2. We count the total size of the state message bundles forwarded by the nodes in an IPN as the load overhead of state information exchange (*i.e.*, if a same bundle is forwarded by multiple nodes, its size contributes to the overhead multiple times).

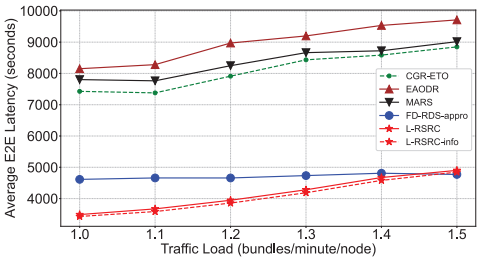

(a) Average E2E latency

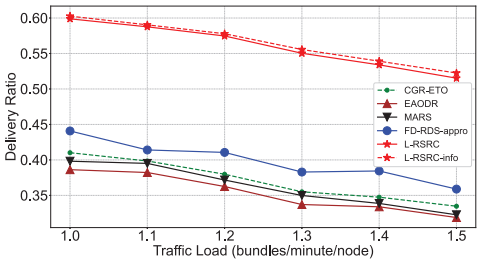

(b) Delivery ratio

Fig. 10. IPN-2 with unexpected interruptions (*Scenario*-1).

We first evaluate the impact of triggering mechanisms by fixing the dissemination mechanism as TTL-1000, *i.e.*, the survival time of each state message bundle is set as $1,000$ seconds. The results obtained in IPN-1 are shown in Fig. 12(a), where "no_info" represents the situation without state information exchange, FTT-200 and FTT-500 are for the FTT mechanisms with state message bundle generation intervals as 200 and 500 seconds, respectively, and QCT-0.01, QCT-0.10 and QCT-0.25 respectively denote the QCT mechanisms

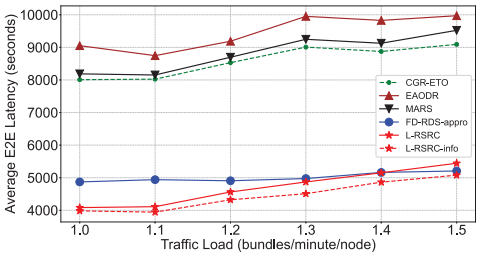

(a) Average E2E latency

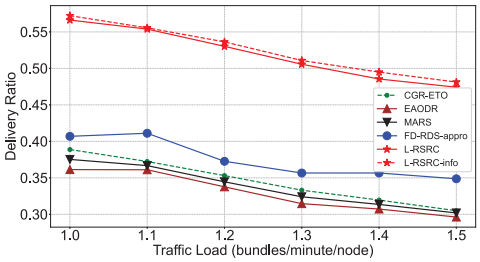

(b) Delivery ratio

Fig. 11. IPN-2 with unexpected interruptions (*Scenario*-2).

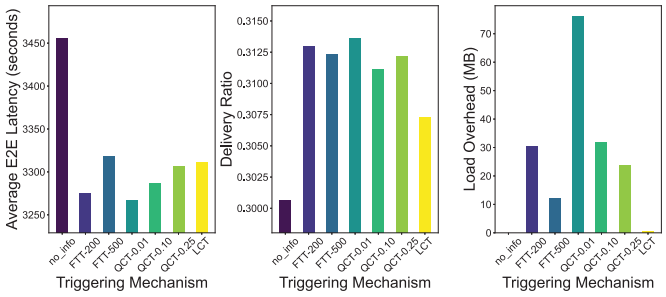

(a) Results with IPN-1

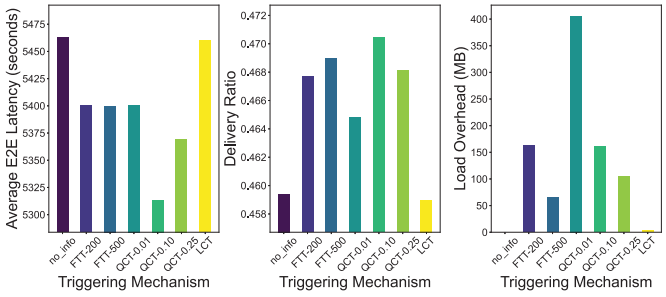

(b) Results with IPN-2

Fig. 12. IP-DT performance under different trigger mechanisms.

with queue length change thresholds as 1%, 10% and 25%, respectively. We have tested more settings for FTT and QCT, but their results exhibit similar trends as those in Fig. 12(a). We can see that although all triggering mechanisms incur load overheads, they achieve certain IP-DT performance gains over the case without state information exchange. Although QCT-0.01 achieves the best IP-DT performance among all the mechanisms, *i.e.*, it provides the shortest average E2E latency and the highest delivery ratio, its load overhead due to state information exchange is also the highest. On the other hand, FTT-200 and QCT-0.10 achieve better balance between IP-DT performance and load overhead. Although the load overhead of LCT is the lowest, it performs worse than most of the FTT and QCT mechanisms on IP-DT routing and scheduling. This is because LCT only cares about link status changes while its extremely low trigger frequency for state message bundle generation cannot report the queue-related information timely.

The results for IPN-2 are shown in Fig. 12(b). This time, QCT-0.10 achieves the best IP-DT performance, and its load overhead is not the highest, while QCT-0.01 does not achieve the best IP-DT performance in IPN-2. This is because the larger and more complex topology of IPN-2 amplifies the negative effect of load overhead, offsetting the gains of QCT-0.01 on IP-DT performance (due to its excessive load overhead).

Next, we evaluate the impact of dissemination mechanisms, and as QCT-0.10 balances the tradeoff between IP-DT performance and load overhead the best in both IPN-1 and IPN-2 according to Fig. 12, we use it as the triggering mechanism. The results obtained in IPN-1 and IPN-2 are shown in Figs. 13(a) and 13(b), respectively. Here, MHC-1 and MHC-2 respectively denote the MHC mechanisms with maximum hop counts as 1 and 2, respectively, and TTL-500, TTL-1000 and TTL-2000 set the survival time of each state message bundle as 500, 1,000 and 2,000 seconds, respectively. We also consider two combined dissemination mechanisms, 1) COM-1: the combination of IDO and MHC-2, and 2) COM-2: the combination of MHC-2 and TTL-2000. In Fig. 13, the IP-DT performance of TTL mechanisms generally improves with the survival time of each state message bundle, but the gain is actually decreasing due to the increase of load overhead, especially for the cases in IPN-2. For instance, in Fig. 13(b), the gains on delivery ratio is relatively small and the average E2E latency even increases, but the load overhead increases dramatically, when comparing TTL-2000 with TTL-1000.

The fact that MHC-2 balances the tradeoff better than MCH-1 suggests that the state information from the nodes other than the neighboring ones contributes to IP-DT decision-making, but at the cost of increased load overhead. It is promising to observe that the performance of IDO in balancing the tradeoff between the average E2E latency and delivery ratio is comparable to that of TTL-500 and TTL-1000 in Figs. 13(a) and 13(b), respectively, while its load overhead is significantly smaller than that of TTL mechanisms. This indicates that the heterogeneity of IPN is better explored by IDO, enabling more efficient limitation of the dissemination range of state message bundles. Moreover, IDO performs better in IPN-2 than in IPN-1, suggesting its better adaptability to larger-sized IPNs. We can see that compared with IDO, the dissemination range of COM-1 is further restricted, resulting in reduced load overhead but slightly degraded IP-DT performance. As for COM-2, its IP-DT performance is better than that of MHC-2 in IPN-1 because of the larger dissemination range, but the increased load overhead leads to decline of IP-DT performance in IPN-2. Fig. 13 suggests that the optimal setting of dissemination mechanism depends on the actual topology and attributes of each IPN, and thus it should be selected empirically.

VI. Conclusion

In this paper, we studied how to leverage the heterogeneity of IPN to improve the performance of IP-DTs. We first

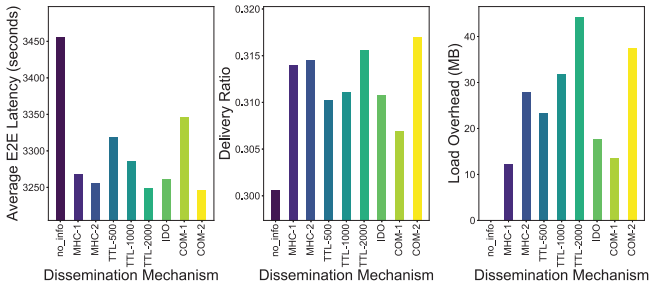

(a) Results with IPN-1

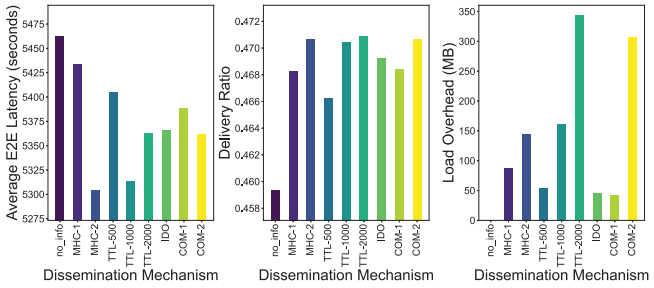

(b) Results with IPN-2

Fig. 13. IP-DT performance under different dissemination mechanisms.

proposed to jointly optimize the routing, scheduling and rate control of IP-DTs on each IPN node, and designed an effective algorithm by leveraging the Lyapunov optimization. Then, we introduced limited state information exchange among IPN nodes, and designed the mechanisms for generating and disseminating the state message bundles, to assist IPN nodes to adjust their routing and scheduling schemes timely in response to unexpected link interruptions and traffic increase. Extensive simulations confirmed the advantages of our proposals over the state-of-the-art, *i.e.*, they not only reduced the average E2E latency but also increased the delivery ratio of IP-DTs.

Acknowledgments

Xiaoliang Chen and Zuqing Zhu are the co-corresponding authors. This work was supported by the National Key R&D Program of China under Grant 2023YFB2903903.

References

[1] I. De Moortel *et al.*, "Roadmap for solar system research 2022," *White Paper, the Science and Technology Facilities Council (STFC)*, Feb. 2023. [Online]. Available: https://www.ukri.org/wp-content/uploads/2022/12/STFC-050123-RoadmapSolarSystemResearch.pdf.

[2] C. Zhou *et al.*, "Scientific objectives and payloads of the lunar sample return mission–chang'e-5," *Adv. Space Res.*, vol. 69, pp. 823–836, Jan. 2022.

[3] C. Li *et al.*, "China's Mars exploration mission and science investigation," *Space Sci. Rev.*, vol. 217, pp. 1–24, May 2021.

[4] T. Bayer *et al.*, "Europa clipper mission: Preliminary design report," in *Proc. of AEROCONF 2019*, pp. 1–24, Jun. 2019.

[5] D. Lauretta *et al.*, "OSIRIS-REx: sample return from asteroid (101955) Bennu," *Space Sci. Rev.*, vol. 212, pp. 925–984, Aug. 2017.

[6] P. Ubertini *et al.*, "Italian report to the 43rd COSPAR scientific assembly," *White Paper*, Jan. 2021. [Online]. Available: https://openaccess.inaf.it/bitstream/20.500.12386/29890/1/ItalianReportCOSPAR2020.pdf.

[7] A. Alhilal, T. Braud, and P. Hui, "The sky is NOT the limit anymore: Future architecture of the interplanetary Internet," *IEEE Aerosp. Electron. Syst. Mag.*, vol. 34, pp. 22–32, Aug. 2019.

[8] M. Marchese, "Interplanetary and pervasive communications," *IEEE Aerosp. Electron. Syst. Mag.*, vol. 26, pp. 12–18, Feb. 2011.

[9] M. Smith *et al.*, "The artemis program: An overview of NASA's activities to return humans to the moon," in *Proc. of AEROCONF 2020*, pp. 1–10, Aug. 2020.

[10] D. Saha *et al.*, "Space microgrids for future manned Lunar bases: A review," *IEEE Open Access J. Power Energy*, vol. 8, pp. 570–583, Sept. 2021.

[11] E. Gibney, "Asteroids, hubble rival and moon base: China sets out space agenda," *Nature*, vol. 603, p. 19, Feb. 2022.

[12] M. Wall. (2016) SpaceX's Elon Musk unveils interplanetary spaceship to colonize Mars. [Online]. Available: https://www.space.com/34210-elon-musk-unveils-spacex-mars-colony-ship.html.

[13] R. Cesarone, D. Abraham, and L. Deutsch, "Prospects for a next-generation deep-space network," *Proc. IEEE*, vol. 95, pp. 1902–1915, Oct. 2007.

[14] Z. Pan *et al.*, "Advanced optical-label routing system supporting multicast, optical TTL, and multimedia applications," *J. Lightw. Technol.*, vol. 23, pp. 3270–3281, Oct. 2005.

[15] Z. Zhu *et al.*, "Jitter and amplitude noise accumulations in cascaded all-optical regenerators," *J. Lightw. Technol.*, vol. 26, pp. 1640–1652, Jun. 2008.

[16] L. Gong *et al.*, "Efficient resource allocation for all-optical multicasting over spectrum-sliced elastic optical networks," *J. Opt. Commun. Netw.*, vol. 5, pp. 836–847, Aug. 2013.

[17] Z. Zhu *et al.*, "Energy-efficient translucent optical transport networks with mixed regenerator placement," *J. Lightw. Technol.*, vol. 30, pp. 3147–3156, Oct. 2012.

[18] W. Lu, Z. Zhu, and B. Mukherjee, "On hybrid IR and AR service provisioning in elastic optical networks," *J. Lightw. Technol.*, vol. 33, pp. 4659–4669, Nov. 2015.

[19] Z. Zhu, W. Lu, L. Zhang, and N. Ansari, "Dynamic service provisioning in elastic optical networks with hybrid single-/multi-path routing," *J. Lightw. Technol.*, vol. 31, pp. 15–22, Jan. 2013.

[20] L. Gong and Z. Zhu, "Virtual optical network embedding (VONE) over elastic optical networks," *J. Lightw. Technol.*, vol. 32, pp. 450–460, Feb. 2014.

[21] P. Lu *et al.*, "Highly-efficient data migration and backup for Big Data applications in elastic optical inter-datacenter networks," *IEEE Netw.*, vol. 29, pp. 36–42, Sept./Oct. 2015.

[22] P. Lu and Z. Zhu, "Data-oriented task scheduling in fixed- and flexible-grid multilayer inter-DC optical networks: A comparison study," *J. Lightw. Technol.*, vol. 35, pp. 5335–5346, Dec. 2017.

[23] J. Liu *et al.*, "On dynamic service function chain deployment and readjustment," *IEEE Trans. Netw. Serv. Manag.*, vol. 14, pp. 543–553, Sept. 2017.

[24] B. Niu *et al.*, "Visualize your IP-over-optical network in realtime: A P4-based flexible multilayer in-band network telemetry (ML-INT) system," *IEEE Access*, vol. 7, pp. 82 413–82 423, Aug. 2019.

[25] B. Mao, X. Zhou, J. Liu, and N. Kato, "On an intelligent hierarchical routing strategy for ultra-dense free space optical low earth orbit satellite networks," *IEEE J. Sel. Areas Commun.*, vol. 42, pp. 1219–1230, May 2024.

[26] B. Mao *et al.*, "On a hierarchical content caching and asynchronous updating scheme for non-terrestrial network-assisted connected automated vehicles," *IEEE J. Sel. Areas Commun., in Press*, 2024.

[27] F. Tang, B. Mao, Y. Kawamoto, and N. Kato, "Survey on machine learning for intelligent end-to-end communication toward 6G: From network access, routing to traffic control and streaming adaption," *IEEE Commun. Surveys Tuts.*, vol. 23, pp. 1578–1598, Aug. 2021.

[28] K. Chin *et al.*, "Energy storage technologies for small satellite applications," *Proc. IEEE*, vol. 106, pp. 419–428, Mar. 2018.

[29] G. Xu and Z. Song, "Effects of solar scintillation on deep space communications: challenges and prediction techniques," *IEEE Trans. Wireless Commun.*, vol. 26, pp. 10–16, Apr. 2019.

[30] G. Araniti *et al.*, "Contact graph routing in DTN space networks: overview, enhancements and performance," *IEEE Commun. Mag.*, vol. 53, pp. 38–46, Mar. 2015.

[31] E. Birrane, S. Burleigh, and N. Kasch, "Analysis of the contact graph routing algorithm: Bounding interplanetary paths," *Acta Astronaut.*, vol. 75, pp. 108–119, Jun./Jul. 2012.

[32] N. Bezirgiannidis, F. Tsapeli, S. Diamantopoulos, and V. Tsaoussidis, "Towards flexibility and accuracy in space DTN communications," in *Proc. of ACM CHANTS 2013*, pp. 43–48, Sept. 2013.

[33] N. Bezirgiannidis *et al.*, "Contact graph routing enhancements for delay tolerant space communications," in *Proc. of ASMS/SPSC 2014*, pp. 17–23, Sept. 2014.

[34] S. El Alaoui and B. Ramamurthy, "EAODR: A novel routing algorithm based on the modified temporal graph network model for DTN-based interplanetary networks," *Comput. Netw.*, vol. 129, pp. 129–141, Dec. 2017.

[35] F. De Rango and M. Tropea, "DTN architecture with resource-aware rate adaptation for multiple bundle transmission in interplanetary networks," *IEEE Access*, vol. 10, pp. 47 219–47 234, Apr. 2022.

[36] S. El Alaoui and B. Ramamurthy, "MARS: A multi-attribute routing and scheduling algorithm for DTN interplanetary networks," *IEEE/ACM Trans. Netw.*, vol. 28, pp. 2065–2076, Oct. 2020.

[37] X. Tian and Z. Zhu, "On the distributed routing and data scheduling in interplanetary networks," in *Proc. of ICC 2022*, pp. 1109–1114, May 2022.

[38] X. Zhou, X. Tian, and Z. Zhu, "Multi-agent DRL for distributed routing and data scheduling in interplanetary networks," in *Proc. of GLOBECOM 2023*, pp. 1–6, Dec. 2023.

[39] X. Tian and Z. Zhu, "On the fine-grained distributed routing and data scheduling for interplanetary data transfers," *IEEE Trans. Netw. Serv. Manag.*, vol. 21, pp. 451–462, Feb. 2024.

[40] S. Dhara, C. Goel, R. Datta, and S. Ghose, "CGR-SPI: A new enhanced contact graph routing for multi-source data communication in deep space network," in *Proc. of SMC-IT 2019*, pp. 33–40, Oct. 2019.

[41] M. Neely, *Stochastic Network Optimization with Application to Communication and Queueing Systems*. San Rafael, CA, USA: Morgan and Claypool, 2010.

[42] S. Burleigh *et al.*, "Delay-tolerant networking: an approach to interplanetary Internet," *IEEE Commun. Mag.*, vol. 41, pp. 128–136, Jun. 2003.

[43] L. Clare, S. Burleigh, and K. Scott, "Endpoint naming for space delay/disruption tolerant networking," in *Proc. of AEROCONF 2010*, pp. 1–10, Apr. 2010.

[44] S. Burleigh, "Interplanetary overlay network: An implementation of the DTN bundle protocol," in *Proc. of CCNC 2007*, pp. 222–226, Jan. 2007.

[45] J. Mukherjee and B. Ramamurthy, "The interplanetary internet implemented on a terrestrial testbed," *Ad Hoc Netw.*, vol. 27, pp. 147–158, Jan. 2015.

[46] J. Burgess *et al.*, "MaxProp: Routing for vehicle-based disruption-tolerant networks." in *Proc. of INFOCOM 2006*, vol. 6, pp. 1–11, Apr. 2006.

[47] I. Bisio, M. Cello, T. De Cola, and M. Marchese, "Combined congestion control and link selection strategies for delay tolerant interplanetary networks," in *Proc. of GLOBECOM 2009*, pp. 1–6, Dec. 2009.

[48] C. Wang *et al.*, "Deep space communication relay services under energy constraint with optimal power control," in *Proc. of GLOBECOM 2013*, pp. 1669–1674, Dec. 2013.

[49] W. Wu, F. Zhou, and Q. Yang, "Adaptive network resource optimization for heterogeneous VLC/RF wireless networks," *IEEE Trans. Commun.*, vol. 66, pp. 5568–5581, Nov. 2018.

[50] E. Uysal-Biyikoglu, B. Prabhakar, and A. El Gamal, "Energy-efficient packet transmission over a wireless link," *IEEE/ACM Trans. Netw.*, vol. 10, pp. 487–499, Aug. 2002.

[51] G. Miao, N. Himayat, Y. Li, and A. Swami, "Cross-layer optimization for energy-efficient wireless communications: a survey," *Wirel. Commun. Mob. Comput.*, vol. 9, pp. 529–542, Apr. 2009.

[52] T. Cover and J. Thomas, *Elements of information theory*. New York: Wiley, 1991.

[53] J. Fraire, O. De Jonckère, and S. Burleigh, "Routing in the space Internet: A contact graph routing tutorial," *J. Netw. Comput. Appl.*, vol. 174, p. 102884, Jan. 2021.

[54] S. Burleigh, K. Fall, and E. Birrane, "RFC 9171: Bundle protocol version 7," *RFC 9171*, Jan. 2022. [Online]. Available: http://tools.ietf.org/html/rfc9171.

[55] Satellite tool kit. [Online]. Available: http://www.agi.com/products/stk/.